Syntheses and magnetic properties of $R_{m+n}Co_{5m+3n}B_{2n}$ compounds

1999 J. Phys.: Condens. Matter 11 8251

(http://iopscience.iop.org/0953-8984/11/42/306)

J. Phys.: Condens. Matter **11** (1999) 8251–8261. Printed in the UK PII: S0953-8984(99)02436-4

Syntheses and magnetic properties of $R_{m+n}Co_{5m+3n}B_{2n}$ compounds

Yi Chen†, J K Liang†‡, X L Chen†, Q L Liu†, B G Shen§ and Y P Shen§

† Institute of Physics and Centre for Condensed Matter Physics, Chinese Academy of Sciences, Beijing 100080, People's Republic of China

‡ International Centre for Materials Physics, Chinese Academy of Sciences, Shengyang, 110015, People's Republic of China

§ State Key Laboratory of Magnetics, Institute of Physics, Chinese Academy of Sciences, Beijing 100080, People's Republic of China

Received 9 March 1999, in final form 18 August 1999

Abstract. New compounds $Pr_3Co_{13}B_2$ and $Nd_5Co_{19}B_6$ have been synthesized successfully. They belong to the $R_{m+n}Co_{5m+3n}B_{2n}$ family with $m = 2$, $n = 1$ and $m = 2$ and $n = 3$, respectively. $Pr_3Co_{13}B_2$ adopts the hexagonal $La_3Ni_{13}B_2$-type structure with lattice parameters $a = 5.0672(3)$ Å and $c = 10.6850(6)$ Å, while $Nd_5Co_{19}B_6$ is isostructural to $Lu_5Ni_{19}B_6$ with $a = 5.1328(3)$ Å and $c = 16.6519(5)$ Å. Magnetic measurements indicate that $Pr_3Co_{13}B_2$ is ferromagnetic with a Curie temperature of 360 K. Its saturation magnetic moment at 5 K is 20.0 μ_B fu^{-1}. Based on the results of the saturation magnetization, two kinds of Co sites with different magnetic moments are proposed. $Pr_3Co_{13}B_2$ exhibits large uniaxial anisotropy with an anisotropy field of 90 A m^{-1} at 5 K. The $Nd_5Co_{19}B_6$ compound is ferromagnetic with a Curie temperature of 380 K. Its saturation magnetic moment and anisotropy field are 21.5 μ_B fu^{-1} and 340 A m^{-1} at 5 K, respectively. No spin reorientation was detected from the temperature dependence of the magnetization of these compounds from 5 K to their Curie temperatures, and the behaviour of magnetocrystalline anisotropy was analysed using the single-ion model.

1. Introduction

It has been known that boron substitution for the Co in RCo_5 (R = rare earth) leads to the formation of a series of compounds expressed by the general formula $R_{1+n}Co_{5+3n}B_{2n}$ [1] ($n = 1, 2, 3, \ldots, \infty$), which is formed by alternate stacking of one layer of RCo_5 and n layers of RCo_3B_2 along the c-axis. Huge anisotropy has been observed in the $Sm_{1+n}Co_{5+3n}B_{2n}$ system. For example, the anisotropy fields of $SmCo_5$, $SmCo_4B$, $Sm_3Co_{11}B_4$ and $SmCo_3B_2$ are found to be 710, 1200, 1160 and 1300 A m^{-1} at 4.2 K, respectively [2]. Although they have uniaxial symmetry, their Curie temperature (T_C) and saturation magnetization (M_S) are too low to be suitable for permanent magnet applications [3–6]. In order to overcome these drawbacks, several attempts have been made to improve the hard magnetic properties by substitutions of Fe for Co or by interstice of nitrogen atoms using the gas–solid reaction modification [7–11]. In our previous papers [12], we demonstrated an alternative strategy, in which we proposed another series of compounds $R_{m+1}Co_{5m+3}B_2$ with high Co content. After we carefully investigated the ternary Nd–Co–B system at relatively low temperature, a new compound $Nd_3Co_{13}B_2$ of the homologous series $R_3Co_{13}B_2$ was discovered. We soon realized that the two homologous series mentioned above can be expressed by a general formula $R_{m+n}Co_{5m+3n}B_{2n}$, which is formed by alternate stacking of m parts of RCo_5 with n parts of RCo_3B_2 along the c-axis. Some of

0953-8984/99/428251+11$30.00

the compositions generated by this formula can be regarded as real compound compositions and we can presume that they have high T_C and M_S due to the high Co content. In the present work, we have extended our study to the R–Co–B systems, and we have found that $Pr_3Co_{13}B_2$ ($m = 2, n = 1$) and $Nd_5Co_{19}B_6$ ($m = 2, n = 3$) can be obtained by vacuum annealing alloy samples at relatively lower temperature; here we report our study on crystal structures and magnetic properties of these intermetallics.

2. Experimental details

Samples were prepared by melting an appropriate amount of raw materials of more than 99.9% purity in an arc furnace. In order to avoid blowing away the lighter pieces of boron under the arc, boron was added through a master alloy of CoB. To ensure the homogeneity of the samples, the ingots were turned upside down and melted several times. The weight loss of the samples during melting was less than 1%. After arc melting, the samples were annealed in vacuum for two months at 873 K and then quenched to room temperature. The x-ray powder diffraction (XRD) data was collected on a Rigaku Rint-2400 diffractometer with Cu K_α radiation and a diffracted beam graphite monochromator, with a scanning step of $2\theta = 0.02^\circ$ and a sampling time of 2 s. The XRD pattern of the sample consisting of powder particles, which were static-magnetically aligned at room temperature, was used to determine the easy magnetization direction (EMD) of this compound. The magnetic properties of the samples were measured by the magnetic balance, vibrating sample magnetometer and superconducting quantum interference device (SQUID).

3. Results and discussion

3.1. $Pr_3Co_{13}B_2$

Single-phase $Pr_3Co_{13}B_2$ results form a peritectoid reaction,

$$PrCo_5 + 2PrCo_4B \leftrightarrow Pr_3Co_{13}B_2.$$

It generally needs prolonged annealing for several weeks at temperatures below 1000 K. Figure 1 shows the XRD pattern for the samples annealed at 600 °C for two months. It can be successfully indexed with a hexagonal cell with lattice parameters $a = 5.0672(3)$ Å and $c = 10.6850(6)$ Å [13]. The space group is $P6/mmm$. An initial structure model was derived from the isostructural $La_3Ni_{13}B_2$ compound and then refined [14] by using the program DBW-9411 [15]. There is one $Pr_3Co_{13}B_2$ formula in a unit cell: Pr atoms are distributed in two different crystallographic sites (1a, 2e), the Co atoms in three different positions (4h, 6i, 3g) and boron in the 2c position. The Rietveld refinement results are shown in figure 1 and table 1. The pattern factor R_P, the weighted pattern factor R_W and the expected pattern factor R_{exp} are 12.1%, 16.8% and 7.8%, respectively. These values are qualitatively good. Finally, the crystal structure of $Pr_3Co_{13}B_2$ is illustrated in figure 2.

Figure 3 shows the magnetic curves at 5 K for the free powder sample of $Pr_3Co_{13}B_2$ measured with a SQUID. The saturation moment of 20.0 μ_B fu^{-1} was derived by fitting the experimental data of $M(H)$ versus H using the law of approach to saturation. For $Pr_3Co_{13}B_2$, in which Pr is a light rare-earth element ($\boldsymbol{J} = \boldsymbol{L} - \boldsymbol{S}$), this implies that the total rare earth moment ($g\boldsymbol{J}\mu_B$) is coupled parallel to the Co moments. Thus, the magnetic moments of $Pr_3Co_{13}B_2$, μ_s can be expressed as

$$\mu_s = 3\langle\mu_{Pr}\rangle + 13\langle\mu_{Co}\rangle \quad (1)$$

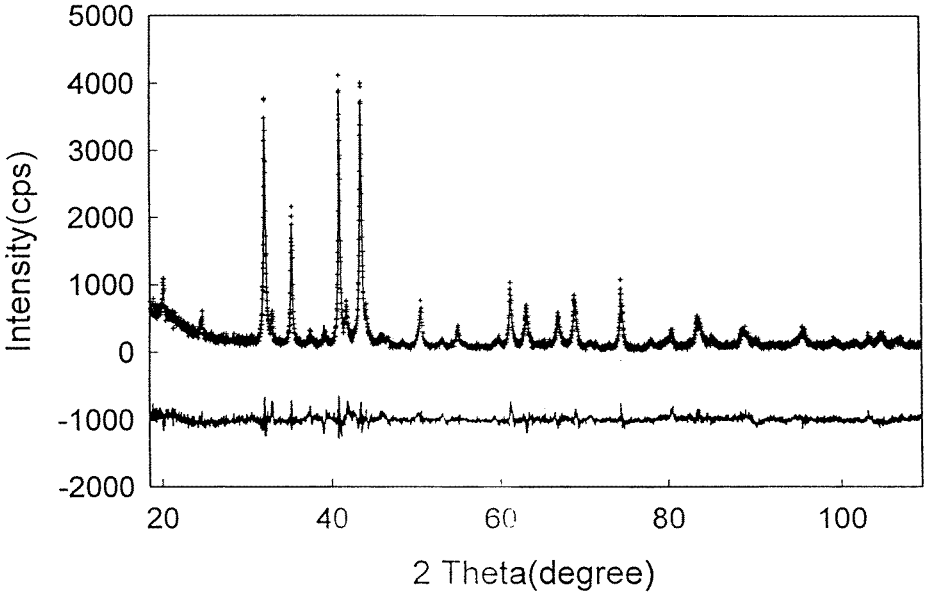

Figure 1. Rietveld analysis of the XRD pattern of $Pr_3Co_{13}B_2$. The observed data are indicated by crosses and the calculated profile by the continuous curve overlaying them. The lower curve is the difference between the observed and calculated intensities at each step plotted on the same scale and shifted a little downwards for clarity.

Table 1. Atomic positions and the lattice parameters of the $Pr_3Co_{13}B_2$ structure obtained from the powder XRD pattern refinement according to the $P6/mmm$ space group.

Atom	Position	x/a	y/b	z/c	The number of neighbour atoms
Pr(1)	1a	0	0	0	6B(1) + 12Co(1)
Pr(2)	2e	0	0	0.3303(5)	6Co(1) + 6Co(2) + 6Co(3)
Co(1)	6i	0.5000	0	0.1341(5)	2Pr(1) + 2Pr(2)
					2Co(2) + 2B(1)
Co(2)	4h	0.3333	0.6667	0.3158(10)	3Co(1) + 3Co(3)
Co(3)	3g	0.5000	0	0.5000	4Pr(2) + 4Co(2)
B(1)	2c	0.3333	0.6667	0	3Pr(1) + 6Co(1)
$z = 1$	$a = 5.0672(3)$ Å		$c = 10.6850(6)$ Å		
$R_p = 12.1\%$	$R_{wp} = 16.8\%$		$R_{exp} = 7.8\%$		

where $\langle\mu_{Pr}\rangle$ and $\langle\mu_{Co}\rangle$ are the average moments of the Pr atoms and Co atoms, respectively. Reliable values of the saturation of moment of cobalt may be obtained only for Gd (s-state) or Y (non-magnetic) compounds in compounds with non-s-state R ions, the Co moment cannot be accurately determined because of the unknown reduction of the R ionic moment by crystal field effects or because of difficulties in saturating the system as a result of its high anisotropy. However, it is possible to estimate the magnetization of the Co sublattice in these systems, provided information is available for the R moments. By assuming the average Pr^{3+} moment to be 2.4 μ_B [3], $\langle\mu_{Co}\rangle$ of 0.98 μ_B is calculated. It is reasonable to assume that the Co atoms at different sites have different magnetic moments. As seen in figure 2, there are three kinds of Co sites expressed by Co(N) with $N = 0$ and 1, where Co(N) means a Co atom which has

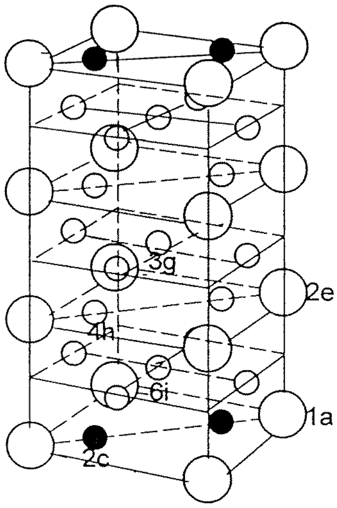

Figure 2. The crystal structure of $Pr_3Co_{13}B_2$. Large open circles are rare earth, small open circles cobalt and full circles boron.

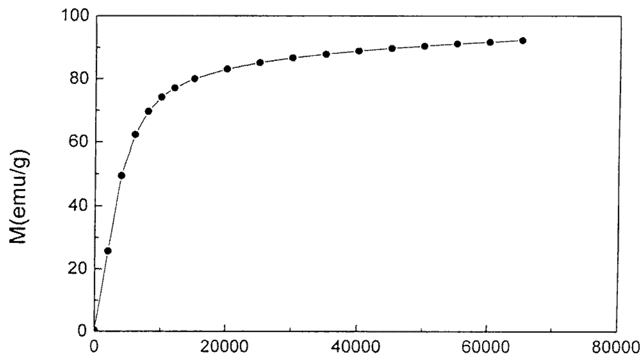

Figure 3. The field dependence of the magnetization curve of the free powder sample of $Pr_3Co_{13}B_2$ measured at 5 K.

NB layers just above or just below it. Thus the average Co moment of $Pr_3Co_{13}B_2$ is expressed by

$$\langle \mu_{Co} \rangle = [4\langle \mu_{Co(0)} \rangle + 3\langle \mu_{Co(0)} \rangle + 6\langle \mu_{Co(1)} \rangle]/13 \tag{2}$$

where $\mu_{Co(N)}$ means the magnetic moment of the Co(N). The near neighbour environment of putting $\mu_{Co(N)}$ at the 4h and 3g positions remains unchanged from the corresponding sites of $PrCo_5$; therefore, $\mu_{Co(0)}$ is assumed to keep the value of 1.3 μ_B [16]. By putting $\mu_{Co(0)}$ and the observed value of $\langle \mu_{Co} \rangle$ into equation (2), 0.6 μ_B is obtained for $\mu_{Co(1)}$. A neutron diffraction study would be quite valuable in determining if these analyses of the magnetic moments are reasonable. We can see that the introduction of B results in a strong decrease of the Co moment. This reduction may occur partly due to simple dilution by B and partly due to a reduction of the Co moment by an electron transfer from B.

Figure 4 shows the temperature dependence of the magnetization, $M(T)$, for the free powder sample of $Pr_3Co_{13}B_2$ in a low field of 0.05 T measured with a SQUID in the

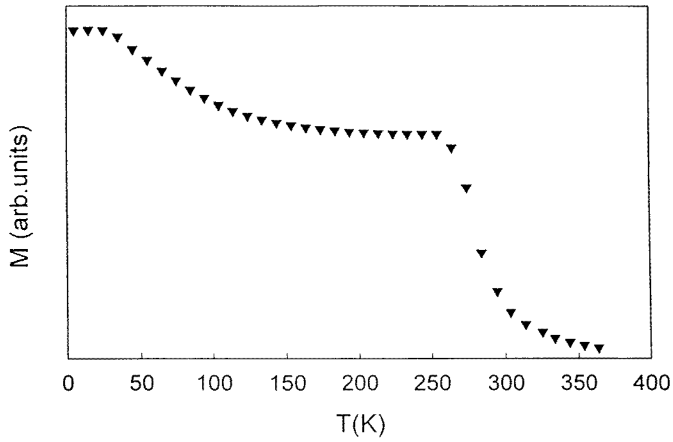

Figure 4. The thermomagnetic curve for the free powder sample of $Pr_3Co_{13}B_2$ in a low field of about 0.05 T.

temperature range below room temperature and with a vibrating sample magnetometer above room temperature. The Curie temperature of 360 K is determined from M^2–T plots by extrapolating M^2 to zero. The Curie temperature of $Pr_3Co_{13}B_2$ is determined from the three different exchange-coupling constants: J_{CoCo}, J_{PrCo} and J_{PrPr}. The Pr–Pr interaction is generally neglected because it is smaller than the Co–Co and Pr–Co interactions. The 3d–4f interaction J_{Pr-Co} has only a minor influence on the Curie temperature. Since the Co–Co exchange-coupling constants are one order of magnitude larger than the Pr–Co exchange-coupling constants, the Curie temperature of $Pr_3Co_{13}B_2$ is mainly determined by the Co–Co interaction. The Curie temperature of $Pr_3Co_{13}B_2$ [17]

$$T_C = \{T_{PrPr} + T_{CoCo} + [(T_{CoCo} - T_{PrPr})^2 + 4T_{PrCo}]^{1/2}\}/2 \tag{3}$$

where the contributive temperature $T_{ii}(i = \text{Pr, Co})$ and T_{PrCo} can be written as

$$T_{ii} = (2A_{ii}Z_{ii}G_i)/(3k_B) \tag{4}$$

and

$$T_{PrCo} = [2A_{PrCo}(Z_{PrCo}Z_{CoPr}G_{Pr}G_{Co})]^{1/2} \tag{5}$$

where $G_i = (g_i - 1)^2 J_i(J_i + 1)$, Z_{ii} is the number of nearest-neighbour j atoms of an i atom, and g_i is the Lande factor of the i atom. The T_C of $Pr_3Co_{13}B_2$ compound is mainly determined by the direct Co–Co exchange interaction and the substitution of B at 2c sites for Co leads to the decrease of the Co–Co exchange interaction. Thus both the magnetic dilution and the decrease of the Co–Co exchange interaction result in a drastic decrease of T_C, as compared to that of the parent compound $PrCo_5$.

Figure 5 illustrates the room-temperature XRD pattern of an unoriented and an oriented sample of $Pr_3Co_{13}B_2$. When a particle has an easy basal plane anisotropy, as confirmed by the reflected x-ray intensity from the plane perpendicular to the applied field, the ($hk0$) intensity increases greatly and the (001) intensity diminishes. When a particle has an easy c-axis anisotropy, the (001) intensity increases greatly and the ($hk0$) intensity diminishes. It can be seen from the oriented sample that the intensity of (003), (005) and (006) are strengthened and the intensity of (110) and (200) are diminished. The results clearly demonstrate that the EMD of $Pr_3Co_{13}B_2$ is parallel to the c-axis. No spin reorientation was detected from the $M(T)$

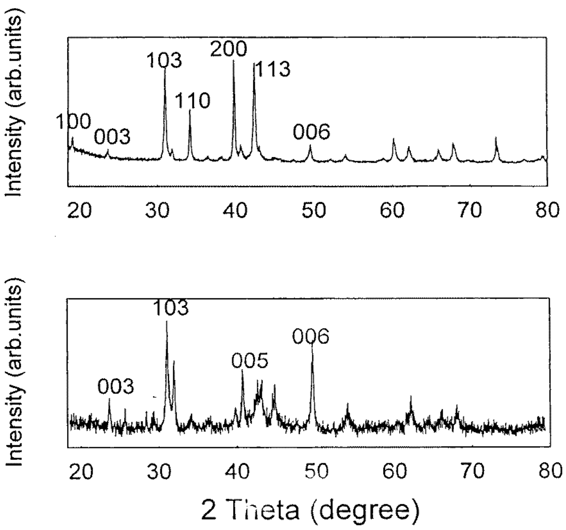

Figure 5. The XRD patterns for sample $Pr_3Co_{13}B_2$ before (a) and after (b) field alignment.

curve (figure 4). This result suggests that the EMD of the $Pr_3Co_{13}B_2$ compound does not change from 5 K to room temperature. In order to measure the magnetocrystalline anisotropy, the static-magnetically aligned sample was then measured with a SQUID and the results are shown in figure 6. By linearly extrapolating ΔM to zero on the ΔM $(=M_{\parallel} - M_{\perp})$–$H$ curve, the anisotropy field H_A of 90 A m^{-1} is derived.

It is well known that the net anisotropy in R–Co compounds is determined by the sum of the R sublattice anisotropy and the Co sublattice anisotropy. In the case of $R_{m+n}Co_{5m+3n}B_{2n}$ compounds

$$K_{1,tot} = (m+n)K_{1,R} + K_{1,Co} \tag{6}$$

where $K_{1,R}$ is the contribution of one R^{3+} ion to the anisotropy constant and $K_{1,Co}$ is the anisotropy constant of the Co sublattice. In the first approximation, $K_{1,R}$ can be described as

$$K_{1,R} = -3\alpha_J A_{20}\langle r_{4f}^2\rangle\langle 3J_{R,z}^2 - J_R(J_R+1)\rangle/2 \tag{7}$$

where α_J is the second-order Stevens coefficient and A_{20} is the second-order crystal electric field (CEF) coefficient. On the basis of a single-ion model [18], the anisotropy of Pr can be described by the product α_J and A_{20}. A negative $\alpha_J A_{20}$ exhibits a uniaxial anisotropy. For $Pr_3Co_{13}B_2$, the contribution of the Pr sublattice to magnetocrystalline anisotropy arises from the coupling between the Pr ion orbit magnetic moment and the crystal electric field. Evidence can be presented to show that A_{20} is negative in the $R_{m+n}Co_{5m+3n}B_{2n}$ compound [19]. The rare earth Pr has a negative α_J: accordingly, the Pr sublattice has an easy planar anisotropy at low temperature. However, under the assumptions of the model of the individual site contributions to anisotropy (ISA) [20], the Co sites of $Pr_3Co_{13}B_2$ related to the 2c site of the RCo_5 structure make large contributions to the magnetocrystalline anisotropy, while the sites $Pr_3Co_{13}B_2$ related to the 3g site of RCo_5 structure make relatively small and reverse contributions. Thus, the total magnetization of the Co sublattice exhibits a uniaxial anisotropy. The axial anisotropy of the Co sublattice overcomes the planar anisotropy of the Pr sublattice, leading to the possibility that $Pr_3Co_{13}B_2$ has its EMD parallel to the c-axis.

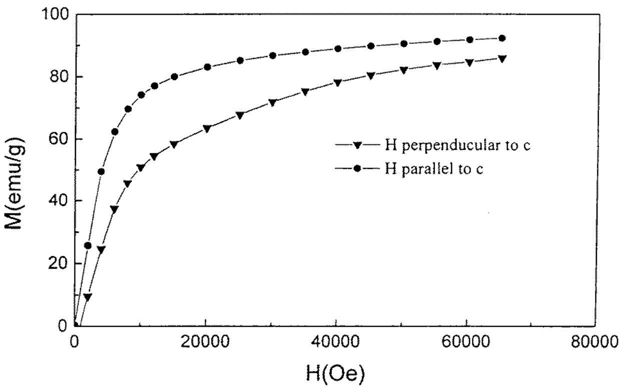

Figure 6. Magnetization as a function of magnetic field at 5 K for the static-magnetically aligned sample of $Pr_3Co_{13}B_2$. The upper curve is parallel to the aligned direction and the lower curve is perpendicular to the aligned direction.

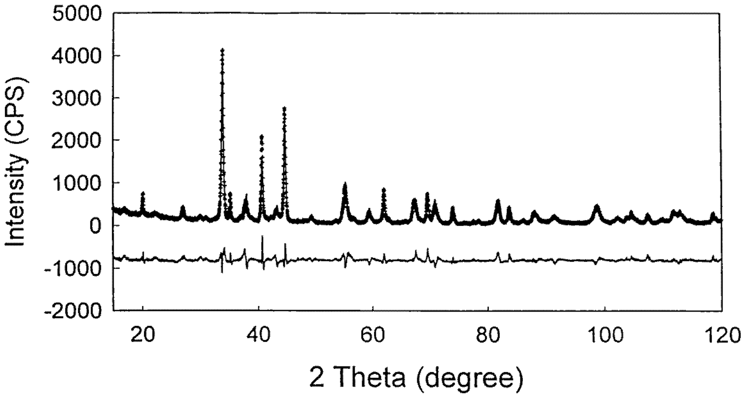

Figure 7. Rietveld analysis of the XRD pattern of $Nd_5Co_{19}B_6$. The observed data are indicated by crosses and the calculated profile by the continuous curve overlaying them. The lower curve is the difference between the observed and calculated intensities at each step.

3.2. $Nd_5Co_{19}B_6$

Single-phase $Nd_5Co_{19}B_6$ results from a peritectoid reaction and the reaction is essentially

$$2NdCo_4B + Nd_3Co_{11}B_4 \leftrightarrow Nd_5Co_{19}B_6.$$

It generally requires prolonged annealing of two months at 873 K. Figure 7 shows its XRD pattern which can be successfully indexed with a hexagonal cell with lattice parameters $a = 5.1328(3)$ Å and $c = 6.659(5)$ Å [13]. The calculated density is $D_x = 8.30$ g cm^{-3}. An initial structure model was derived from the isostructural $Lu_5Ni_{19}B_6$ based on the space group $P6/mmm$. There is one $Nd_5Co_{19}B_6$ formula unit in the cell: the Nd atoms occupy three different crystallographic sites (1b, $2e_1$, $2e_2$), the Co atoms four different positions ($4h_1$, $6i_1$, $6i_2$, 3f) and B the 2d and $4h_2$ positions. The Rietveld refinement [14, 15] was performed and the results are shown in figure 7 and table 2. The residual agreement factors of R_P, R_W and R_{exp} are 13.6%, 17.3% and 6.9%, respectively, and these values are qualitatively good. The crystal structure of $Nd_5Co_{19}B_6$ is illustrated in figure 8.

Table 2. Atomic positions and the lattice parameters of the $Nd_5Co_{19}b_6$ structure obtained from the powder XRD refinement according to the $P6/mmm$ space group.

Atom	Position	x/a	y/b	z/c
1Nd	1b	0	0	0.5000
2Nd	$2e_1$	0	0	0.0964(1)
2Nd	$2e_2$	0	0	0.2976(1)
4Co	$4h_1$	0.3333	0.6667	0.2955(2)
6Co	$6i_1$	0.5000	0	0.1742(1)
6Co	$6i_2$	0.5000	0	0.4114(1)
3Co	3f	0.5000	0	0.0000
2B	2d	0.3333	0.6667	0.5000
4B	$4h_2$	0.3333	0.6667	0.0936(16)
$z = 1$	$a = 5.1328(3)$ Å		$c = 16.6519(5)$ Å	
$R_p = 13.6\%$	$R_{wp} = 17.3\%$		$R_{exp} = 6.9\%$	

Figure 9 shows the magnetic isotherm at 5 K for the free powder sample of $Nd_5Co_{19}B_6$ measured with a SQUID magnetometer. The saturation moment of 21.5 μ_B fu^{-1} was derived by fitting the experiment data of $M(H)$ versus H using the law of approach to saturation. For $Nd_5Co_{19}B_6$, in which Nd is a light rare-earth element ($\boldsymbol{J} = \boldsymbol{L} - \boldsymbol{S}$) this implies that the total rare-earth moment ($g\boldsymbol{J}\mu_B$) is coupled parallel to the Co moments. Thus, the magnetic moments of $Nd_5Co_{19}B_6$, μ_s, can be expressed as

$$\mu_s = 5\langle\mu_{Nd}\rangle + 19\langle\mu_{Co}\rangle \tag{8}$$

where $\langle\mu_{Nd}\rangle$ and $\langle\mu_{Co}\rangle$ are the average moments of Nd atoms and Co atoms, respectively. By assuming the average Nd^{3+} moment to be 3 μ_B, $\langle\mu_{Co}\rangle$ of 0.34 μ_B is calculated. We can see that the introduction of B atoms results in a small value of the Co moment. This might be understood in terms of 2p–3d hybridization. Band-structure calculations [12] have revealed that the p–d hybridization lowers the density of states at the Fermi level and reduces the 3d-band splitting when B atoms preferentially substitute into the nearest-neighbour sites of the Nd atoms.

Figure 10 shows the temperature dependence of the magnetization, $M(T)$, for the free powder sample of $Nd_5Co_{19}B_6$ in a low field of 0.05 T measured with a SQUID in the temperature range below room temperature and with a vibrating sample magnetometer above room temperature. The Curie temperature of 380 K is determined from M^2–T plots by extrapolating M^2 to zero. The T_C of the $Nd_5Co_{19}B_6$ compound is mainly determined by the direct Co–Co exchange interaction and the substitution of B at the 2c and $4h_2$ sites for Co leads to the decrease of the Co–Co exchange interaction. Thus both the magnetic dilution and the decrease of the Co–Co exchange interaction result in a drastic decrease of T_C, as compared to that of the parent compound $NdCo_5$. No spin reorientation was detected from the $M(T)$ curve. This result suggests that the EMD of the $Nd_5Co_{19}B_6$ compound does not change from 5 K to its Curie temperature.

Figure 11 illustrates the room-temperature XRD pattern of an unoriented and an oriented sample of $Nd_5Co_{19}B_6$. It can be seen that the pattern of the oriented sample contains the peaks of (200) and (110). The result clearly demonstrates that the EMD of $Nd_5Co_{19}B_6$ lies in the basal plane. In order to measure the magnetocrystalline anisotropy (MCA), the rotation-magnetically aligned sample was measured with a SQUID and the result is shown in figure 9. By linearly extrapolating ΔM to zero on the $\Delta M(=M - M)$–H curve, the anisotropy field H_A 340^{-1} A m^{-1} is derived. The net anisotropy in $Nd_5Co_{19}B_6$ is determined by the

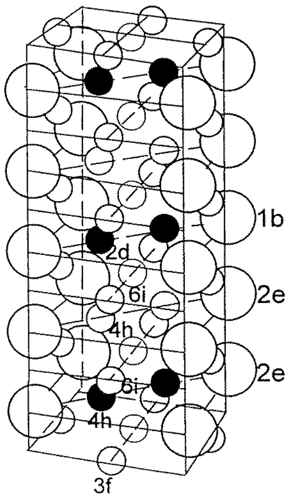

Figure 8. The crystal structure of $Nd_5Co_{19}B_6$. Large open circles are rare earth, small open circles cobalt and full circles boron.

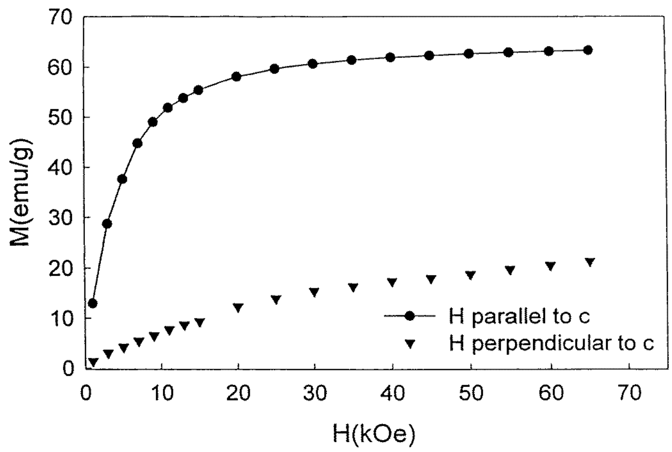

Figure 9. The isotherm at 5 K for $Nd_5Co_{19}B_6$ with the external applied field either parallel or perpendicular to the alignment direction of the rotation-magnetically aligned sample.

sum of the Nd sublattice anisotropy and the Co sublattice anisotropy. The contribution of the Nd sublattice to magnetocrystalline anisotropy arises from the coupling between the Nd ion orbital magnetic moment and the crystal electric field. The Nd sublattice plays a more important role in determining the EMD at low temperature compared with the Co sublattice. As mentioned above, A_{20} is negative in $R_{m+n}Co_{5m+3n}B_{2n}$ compounds [19]. The rare earth Nd has a negative α_J: accordingly, $Nd_5Co_{19}B_6$ has an easy planar anisotropy at low temperature. On the other hand, under the assumptions of the model of ISA [20], the Co sites in $Nd_5Co_{19}B_6$ related to the 2c site in the RCo_5 structure make large contributions to the magnetocrystalline anisotropy, while the Co sites related to the 3g site in the RCo_5 structure make relatively small and reverse contributions. Compared to $Pr_3Co_{13}B_2$, more non-magnetic B atoms substitute for

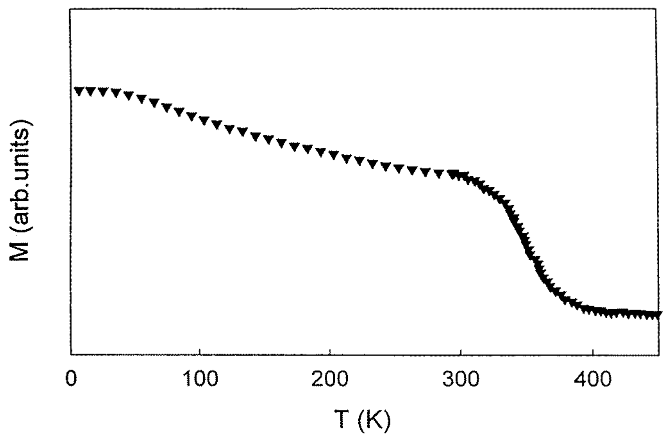

Figure 10. The thermomagnetic curve for the free powder sample of $Nd_5Co_{19}B_6$ in a low field of about 0.05 T.

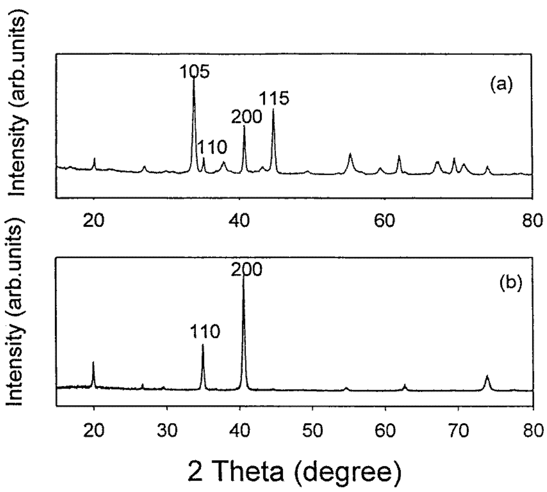

Figure 11. The XRD patterns for sample $Nd_5Co_{19}B_6$ before (a) and after (b) field alignment.

Co atoms at the sites (2d and $4h_2$) related to the 2c site in the RCo_5 structure, and this implies that $Nd_5Co_{19}B_6$ has its EMD in the basal plane at all temperatures.

4. Conclusion

New compounds $Pr_3Co_{13}B_2$ and $Nd_5Co_{19}B_6$ with high Co content were synthesized. They are members of the homologous series $R_{m+n}Co_{5m+3n}B_{2n}$ with $m = 2, n = 1$ and $m = 2, n = 3$, respectively. The $Pr_3Co_{13}B_2$ compound is ferromagnetic with a Curie temperature of 360 K. Its saturation magnetic moment is 20.0 μ_B fu^{-1} and the anisotropy field is 90 A m^{-1} at 5 K. The average Co moments of the $Pr_3Co_{13}B_2$ compound are expressed by $\langle\mu_{Co}\rangle = [4\langle\mu_{Co(0)}\rangle + 6\langle\mu_{Co(1)}\rangle + 3\langle\mu_{Co(0)}\rangle]/13$, where $\mu_{Co(N)}$ means the magnetic moment of Co with N layers of B just above or just below it. The introduction of B results in a strong decrease of the Co moment: $\mu_{Co(0)}$ and $\mu_{Co(1)}$ are 1.3 μ_B and 0.6 μ_B, respectively. The $Nd_5Co_{19}B_6$ compound is ferromagnetic with a Curie temperature of 380 K. Its saturation magnetic moment is 21.5 μ_B fu^{-1} and the anisotropy field is 340 A m^{-1} at 5 K. No spin reorientation was detected from the temperature dependence of the magnetization of these compounds. We believe that many intermetallic compounds of the $R_{m+n}Co_{5m+3n}B_{2n}$ family with different m and n are yet to be found at relatively low temperature, and such a systematic investigation may prove to be fruitful.

Acknowledgments

This work was supported by the National Natural Science Foundation of China and the State Key Project for Fundamental Research in China. Yi Chen wishes to express his gratitude to J L Wang and N Tang for their assistance in the magnetic parameter measurements and to Xiang Li for her help during the experiment.

References

[1] Ku'zma Yu B and Bilonizhko N S 1973 *Kristallografiya* **18** 710
[2] Ido H, Sugiyama K, Hachino H, Date M, Cheng S F and Maki K 1992 *Physcia* B **177** 265
[3] Pedziwatr A T, Jiang S Y, Wallace W E, Burzo E and Pop V 1987 *J. Magn. Magn. Mater.* **66** 69
[4] Tetean R and Burzo E 1996 *J. Magn. Magn. Mater.* **157/158** 633
[5] Ito T, Asano H, Ido H and Yamada M 1996 *J. Appl. Phys.* **79** 5507
[6] Kowalcyk A 1997 *J. Magn. Magn. Mater.* **175** 279
[7] Nadia A E and Standelmaler H H 1983 *Z. Mettallkde.* **74** 86
[8] Huang M Q, Ma B M, Zhang L Y, Wallace W E and Sankar S G 1990 *J. Appl. Phys.* **67** 4981
[9] Huang M Q, Ma B N, Cheng S F and Wallace W E 1991 *J. Appl. Phys.* **69** 5599
[10] Ido H, Ogata H and Maki K 1993 *J. Appl. Phys.* **73** 6269
[11] Ido H, Nashima O, Takahashi T, Oda K and Sugiyama K 1994 *J. Appl. Phys.* **76** 6165
[12] Chen Y, Liu Q L, Liang J K, Chen X L, Shen B G and Huang F 1999 *Appl. Phys. Lett.* **74** 856
[13] Werner P E 1964 *Z. Kristallogr.* **120** 375
Werner P E 1976 *J. Appl. Crystallogr.* **9** 216
[14] Rietveld H M 1967 *Acta Crystallogr.* **229** 151
Rietveld H M 1969 *J. Appl. Crystallogr.* **2** 65
[15] Young R Y, Sakthirel A, Moss T S and Paiva-Santos C O 1995 *J. Appl. Crystallogr.* **28** 366
[16] Velge W A J J and Buschow K H J 1968 *J. Appl. Phys.* **39** 1717
[17] Mohn P and Wohlfarth E P 1987 *J. Phys. F: Met. Phys.* **17** 2424
[18] Buschow K H J 1991 *Rep. Prog. Phys.* **54** 1123
[19] Smit H H, Thiet R C and Buschow K H J 1988 *J. Phys. F: Met. Phys.* **18** 295
[20] Streever R L 1979 *Phys. Rev.* B **19** 2704